Mg coordination in a MgSiO3 glass using neutron diffraction coupled with isotopic substitution

L. Cormier, G. J. Cuello

Mg coordination in a MgSiO₃ glass using neutron diffraction coupled with isotopic substitution

L. Cormier[1,*] and G. J. Cuello[2]

[1]*Institut de Minéralogie et de Physique des Milieux Condensés, Université Pierre et Marie Curie, CNRS UMR 7590,*
Université Paris Diderot, IPGP, 140 rue de Lourmel, F-75015 Paris, France
[2]*Institut Laue-Langevin, 6 rue Jules Horowitz, BP 156, F-38042 Grenoble cedex 9, France*

Neutron diffraction with isotopic substitution (^{25}Mg/^{nat}Mg) is used to investigate the Mg environment in MgSiO₃ glass. The neutron-diffraction data are coupled with x-ray diffraction and a reverse Monte Carlo modeling. The Mg environment can be fully resolved from other contributions. We show that two Mg-O contributions are present at ∼1.99 ± 0.01 Å and 2.21 ± 0.01 Å, with an average coordination number of 4.5 ± 0.1 O neighbors around Mg. These distorted Mg sites participate in an inhomogeneous distribution of Mg atoms. This organization results from the liquid state and has implications in understanding the immiscibility gap and glass forming ability.

I. INTRODUCTION

MgO is an oxide incorporated in technological glasses and fibers and bioactive glasses[1−4] due to its strong influence on the structural and physical properties of silicate glasses, such as elastic properties, densities, and viscosities.[4−6] Furthermore, Mg-rich crystalline or amorphous silicates are major components of the earth mantle and interplanetary dust.[7−9] The Mg environment is of prime importance to interpret dynamic and physical properties such as crystallization, partitioning of elements, diffusion, and viscosity. Metasilicate glasses have the particularity of containing the lowest SiO₂ content, which allows the formation of an infinite framework.[10] The role of Mg atoms in such glasses is ambiguous between modifier and network former, and can lead to the formation of invert glasses when MgO content exceeds the SiO₂ one.[11]

The coordination of Mg for an enstatite glass composition (MgSiO₃) has been the subject of numerous investigations. X-ray diffraction data have been interpreted considering a distorted octahedral environment (4 O neighbors at 2.08 Å and 2 O neighbors at 2.50 Å)[10] or a tetrahedral environment with a mean distance $d_{Mg-O} = 2.04$ Å.[12] Using a ^{25}Mg NMR, sixfold environment is mainly proposed with possible fivefold sites.[13−15] Wilding *et al.*[16] have recently reported an average coordination number of 4.5 by coupling x-ray and neutron diffraction with a reverse Monte Carlo (RMC) simulation. A similar study gives a higher coordination of 5.1.[17] These two diffraction investigations suggest a mixture of MgO₄ and MgO₅ polyhedra, which are connected to the silicate network by corner sharing with SiO₄ tetrahedra.[18] Molecular dynamics (MD) calculations also indicate a wide range of environments. Early MD studies indicated tetrahedral coordination with a Mg-O distance of 1.9−1.96 Å,[19] while Kubicki and Lasaga predict that Mg resides in a distorted site, with 4.3 O atom neighbors near 2 Å and two more near 2.2 Å,[20] in agreement with a recent MD simulation that indicated distorted MgO₆ octahedra with an average Mg-O distance of 2.07 Å and a coordination of 5.7.[21]

Despite all these experimental and theoretical studies, the local Mg environment is not ascertained unambiguously and exhibits a wide range of coordination, the possibility of irregular polyhedra, and a mixture between different sites. The difficulties of accurately determining the coordination come from the low natural abundance of ^{25}Mg and large nuclear quadrupole interactions for ^{25}Mg NMR, the site distortion that leads to an underestimate of the distant neighbors for extended x-ray-absorption fine structure (EXAFS) data or the overlapping with other contributions, especially for x-ray diffraction for which Mg is a relatively weak x-ray scatterer.

A possible method of isolating the cation environment is neutron diffraction with isotopic substitution (NDIS).[22,23] In this contrast method, a difference function separates the environment for a substituted cation from the other contributions. This technique has been successfully applied to Ca in a CaSiO₃ glass,[24,25] allowing the determination of the Ca-O environment that is usually overlapping with the O-O contribution in x-ray or neutron-diffraction data. An advantage of NDIS is the ability to obtain additional information on the medium-range order (>3 Å) around the substituted element. In the case of Mg, there is a suitable difference between the neutron scattering length of ^{25}Mg, $b_{25Mg} = 3.62$ fm, and Mg in its natural abundance (^{nat}Mg), $b_{natMg} = 5.37$ fm.

We have applied NDIS to MgSiO₃ using the ^{nat}Mg/^{25}Mg substitution. The first Mg-O contribution can be fully separated from other contributions, allowing an exact determination of the Mg coordination number. To determine the glass structure in detail, we have performed structural modeling by employing the reverse Monte Carlo (RMC) simulation technique. By coupling neutron and x-ray diffraction with RMC modeling, we have resolved completely the Mg environment, its distribution, and its connection with the silicate network.

II. EXPERIMENT

A. Sample preparation

Two MgSiO₃ glasses were prepared: the first sample was enriched with ^{25}MgO (98.79%) and the second one with ^{nat}MgO. The dried starting materials (MgO, SiO₂) were ground together, melted in air within a Pt-10%Rh crucible at 1650 °C, and then quenched by putting the bottom of the crucible into water. All samples were grounded and remelted twice to ensure a homogeneous glass. Glass compositions were determined using an electron microprobe microanalyser (CAMECA

TABLE I. Composition (mol %, ±0.05), density (g cm^{-3}, ±0.02) and atomic number density ρ (at Å^{-3}, ±0.003) for the silicate glasses.

Glass sample	SiO$_2$	MgO	Density	ρ
^{25}MgSiO$_3$	50.84	49.16	2.70	0.0804
^{nat}MgSiO$_3$	50.38	49.62	2.69	0.0807

SX50) at the Camparis Centre (University Pierre et Marie Curie, France). Glass densities were determined in toluene using the Archimedes' principle. The chemical compositions, densities, and notation of the studied glasses are reported in Table I.

B. Neutron diffraction

Neutron-diffraction data were collected at room temperature using the D4c Diffractometer at the Institut Laue-Langevin.[26] Glass powders (∼5 g) were loaded into a cylindrical vanadium can of 6 mm in diameter. A group of nine detectors, each with an 8° angular range and separated from the adjacent ones by 7°, were used. The diffracted intensities at five detector positions are recorded, which allow a continuous measurement over the 1.3−140° angular range and limit the effect of the relative cell efficiencies. The incoming wavelength was 0.497 Å, giving a total scattering vector (Q) range of 0.3−23.6 Å^{-1} ($Q = 4\pi \sin\theta/\lambda$, with θ the diffraction angle and λ the incoming wavelength). Data corrections include detector efficiency, background and container scattering, absorption, multiple scattering, inelastic effects, and normalization from a vanadium standard to obtain the structure factor $F^N(Q)$. The notation for the structure factors and correlation functions are explained in previous papers.[27−29]

The total structure factor for neutron diffraction is defined as

$$F^N(Q) = \sum_{i,j} c_i c_j \bar{b}_i \bar{b}_j [F_{ij}(Q) - 1], \qquad (1)$$

with c_i and $\bar{b}_i$ as the atomic concentration and the coherent scattering length, respectively, for species i, and $F_{ij}(Q)$ as the partial structure factor for the correlation between atoms i and j. The correlation function $D^N(r)$ is obtained by Fourier transform of the total structure factor:

$$D^N(r) = \frac{2}{\pi} \int_0^\infty Q \, F(Q) \, \sin(Qr) \, dQ. \qquad (2)$$

The $D^N(r)$ function is a sum of the partial pair distribution functions (PPDFs), $g_{ij}(r)$, corresponding to the correlations between atoms i and j:

$$D^N(r) = 4\pi r \rho_0 \sum_{i,j} c_i c_j \bar{b}_i \bar{b}_j [g_{ij}(r) - 1], \qquad (3)$$

where ρ_0 is the atomic number density.

By changing the magnesium isotopic content, the Mg coherent scattering length differs between the two samples, $\bar{b}_{25} = 4.151$ fm and $\bar{b}_{nat} = 5.375$ fm, according to the isotopic content of the starting MgO oxides. Therefore, their total structure factors, $F^{25}(Q)$ and $F^{nat}(Q)$, are different by

an amount $\Delta F^{Mg}(Q) = F^{nat}(Q) - F^{25}(Q)$. Assuming that the structure of the two glasses is equivalent, the $\Delta F^{Mg}(Q)$ function contains only the partial structure factors involving Mg:[22,23]

$$\Delta F^{Mg}(Q) = \sum_{i \neq Mg} 2 c_i c_{Mg} \bar{b}_i (\bar{b}_{nat} - \bar{b}_{25})[F_{iMg}(Q) - 1]$$
$$+ c_{Mg}^2 (\bar{b}_{nat}^2 - \bar{b}_{25}^2)[F_{MgMg}(Q) - 1]. \qquad (4)$$

The Fourier transform of $\Delta F^{Mg}(Q)$ gives the Mg-centered correlation function, $\Delta D^{Mg}(r)$, expressed as

$$\Delta D^{Mg}(r) = 4\pi r \rho_0 \Bigg[\sum_{i \neq Mg} 2 c_i c_{Mg} \bar{b}_i (\bar{b}_{nat} - \bar{b}_{25})[g_{iMg}(r) - 1]$$
$$+ c_{Mgi}^2 (\bar{b}_{nat}^2 - \bar{b}_{25}^2)[g_{MgMg}(r) - 1] \Bigg]. \qquad (5)$$

C. X-ray diffraction

X-ray diffraction data were collected with a diffractometer (PANalytical X'Pert PRO) operating with a Mo Kα radiation (λ=0.7093 Å). The angular range $2° < 2\theta < 148°$ for the measurements corresponds to the Q range from 0.3 to 17 Å^{-1}. Data were corrected for polarization and absorption, Compton scattering and normalized, using the Krogh-Moe-Norman method,[30] to obtain the total structure factor for x-ray diffraction $F^X(Q)$ defined as

$$F^X(Q) = \sum_{i,j} c_i c_j f_i(Q) f_j(Q) [F_{ij}(Q) - 1] \Bigg/ \left(\sum_i c_i f_i(Q) \right)^2, \qquad (6)$$

where $f_i(Q)$ is the Q-dependant x-ray scattering factor. The correlation function $D^X(r)$ is obtained by Fourier transform of the total structure factor [with a modification function $\exp(-\alpha Q^2)$ and α=0.005 Å^2]. The expression of $D^X(r)$ differs from $D^N(r)$ because the PPDFs are convoluted with the Fourier transform of the x-ray scattering factors $f_i(Q)$:[31,32]

$$D^X(r) = 4\pi \rho_0 \{[r(g_{ij}(r) - 1)] \otimes FT(f_{ij}(Q))\}, \qquad (7)$$

where $f_{ij}(Q) = f_i(Q) f_j(Q)/[\sum_i c_i f_i(Q)]$.

III. EXPERIMENTAL RESULTS

The experimental structure factors are shown in Fig. 1 for x-ray and neutron-diffraction data. The difference function $\Delta F^{Mg}(Q)$, giving the Mg environment, is also shown in Fig. 1(b). The real-space distribution functions are plotted in Fig. 2 for x-ray and neutron diffraction. X-ray diffraction data are sensitive to Si and Mg environments. The first three peaks can be ascribed to Si-O (1.62 ± 0.01 Å), Mg-O (2.05 ± 0.01), and Si-Si (3.16 ± 0.01 Å) correlations.[10,12] The peak at 3.1 Å has a shoulder most likely due to O-O correlations. Above 3.5 Å, there is an overlap between the different contributions and information on the medium-range order is limited. Neutron-diffraction data are dominated by correlations involving Mg and O. Since the neutron structure factors extend to high-Q values, the spatial resolution is
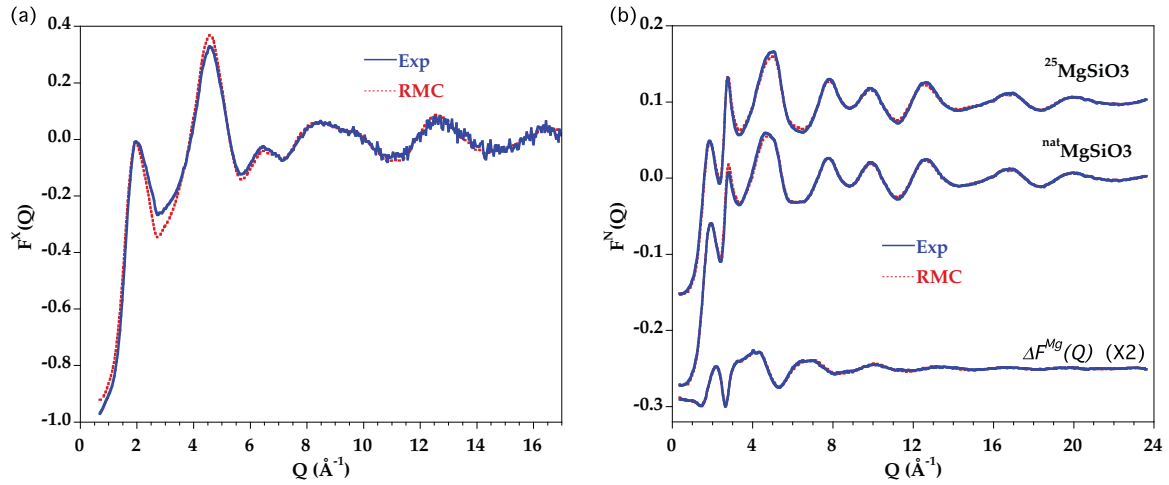
FIG. 1. (Color online) Comparison between the experimental structure factors (solid lines) and those calculated from the RMC model (dotted lines) for (a) x-ray and (b) neutron diffraction. The neutron-diffraction data are for the two samples containing ^{25}Mg or ^{nat}Mg, and for the difference $\Delta F^{Mg}(Q)$.

improved in real space compared to x-ray diffraction data. This can be seen by the Mg-O contribution around 2 Å, which is almost completely separated from the other contributions and exhibits a shoulder at high-r values, indicating that two Mg-O contributions are involved. Wilding *et al.* have also previously noted this asymmetry with a significant tail to high r.[16] The peak at 2.66 Å is due to the O-O contributions. Broad features extending up to 15 Å evidence the medium-range organization. The difference function allows the separation of all the Mg-centered PPDFs and, thereby, the complete determination of the Mg site. Distinct contributions can be seen between 3 and 5 Å, and further broad contributions are discernible up to 10 Å. The interpretation of these features requires the recourse to atomic modeling.

Direct quantitative information can be obtained by Gaussian fitting of the data. We used a procedure previously described where the Gaussian function is convoluted with the Fourier transform of a modification function (a step function in the present study) to take fully into account the truncation effects of the Fourier transform due to the limitation of the data in Q space.[33] The results of the Gaussian fits up to 3 Å are presented in Fig. 3 and the fitted parameters are summarized in Table II, with R as the interatomic distances, CN as the coordination number, and σ as the standard deviation. The first peak at 1.621 Å is consistent with the presence of SiO₄ tetrahedra. The Mg-O contributions need to be fitted with two contributions at 1.99 and 2.21 Å, suggesting the presence of several cationic sites. The difference function gives a complete deconvolution from the Si-O or O-O contributions, allowing a full extraction of the Mg-O contributions and thus an exact evaluation of the Mg environment. An average coordination number of 4.50 ± 0.02 is obtained. Although two Mg-O contributions can be determined, it is not possible to ascribe their origin to four-, five-, or sixfold coordinated sites. Modeling of the data can
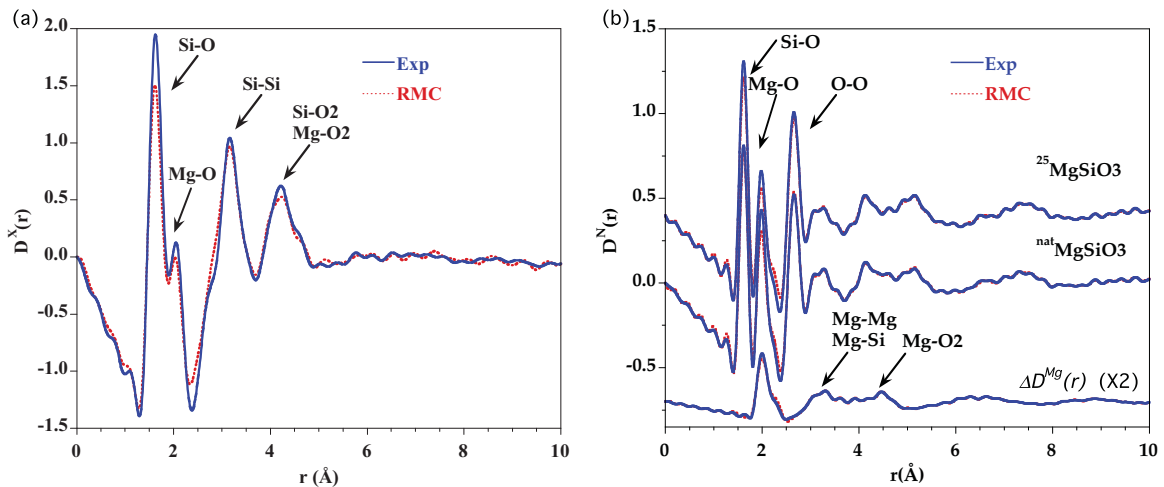

FIG. 2. (Color online) Experimental total correlation functions (solid lines) compared with those obtained from the RMC model (dotted lines), calculated by Fourier transform of the total structure factors for (a) x-ray and (b) neutron diffraction. The neutron-diffraction data are for the two samples containing ^{25}Mg or ^{nat}Mg, and for the difference $\Delta D^{Mg}(r)$.
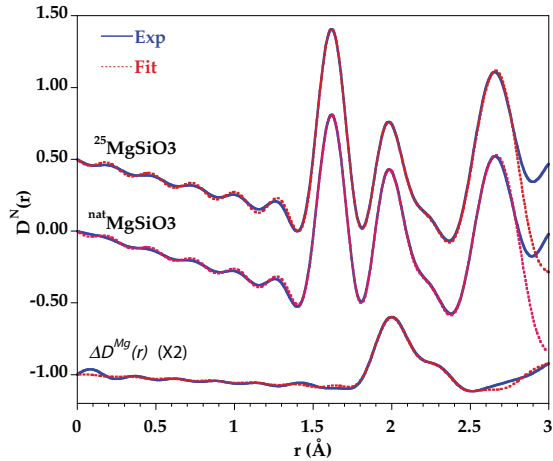
FIG. 3. (Color online) Gaussian fitting of the neutron-diffraction data for the total correlation functions corresponding to the ^{25}MgSiO$_3$ and ^{nat}MgSiO$_3$ glasses (two upper curves) and for the difference correlation function $\Delta D^{Mg}(r)$.

provide relevant information on this local order as well as on the medium-range organization.

IV. REVERSE MONTE CARLO MODELING

A molecular dynamics (MD) simulation was performed to give the starting configuration for the reverse Monte Carlo (RMC) procedure, which provides more reliable models than those obtained by standard hard-sphere modeling.[34] The calculations were performed in the microcanonical (NVE) ensemble using the DL_POLY code.[35,36] The interaction potential and parameters have been previously reported[37] and applied to a box of 4000 atoms with the experimental density. The liquid was equilibrated at high temperature (3000 K during 100 000 steps of 1 fs) and then cooled down to 300 K with a cooling rate of 10^{13} K/s. The final configuration obtained by MD serves as the starting one in the RMC procedure.

The RMCA code was used for the RMC modeling,[38,39] using constraints on the closest atom-atom distances (values can be found in Ref. [17]) and keeping Si atoms in tetrahedral sites. No constraints were imposed on the Mg environment, but it was strongly constrained by the experimental difference neutron function $\Delta F^{Mg}(Q)$. Total x-ray and neutron structure factors [i.e., $F^X(Q)$, $F^{25}(Q)$, $F^{nat}(Q)$, and $\Delta F^{Mg}(Q)$] were used during the RMC modeling process. Given the lowest Q range and signal-to-noise ratio, higher discrepancies for x-ray data were allowed with the measured structure factors. The $F(Q)$ and $D(r)$ functions derived from the RMC models are plotted in Figs. 1 and 2 as dotted lines. The $D(r)$ functions

were obtained by Fourier transform of the simulated structure factors in exactly the same way as the experimental data to allow a direct comparison. The factor of agreement (i.e., the square difference between the measured and calculated structure factors) is typically 5×10^{-5} for the total neutron structure factors when starting with the MD model, and it is improved to 6.5×10^{-6} after the RMC procedure. The topology of the MD model is not strongly modified but the changes allow a quantitative reproduction of the diffraction data. The partial structure factors and partial distribution functions are shown in Fig. 4 for both the initial MD simulation and after the RMC procedure. We can note small but significant differences after the RMC modeling, including a decrease of the mean Si-O, Si-Si, and Si-Mg first contribution, and a better-defined O-O contribution at 2.6 Å. The main changes appear for the Mg-O pair revealing the influence of the $\Delta F^{Mg}(Q)$ function: the intensity of the first Mg-O peak is increased and slightly shifted to lower-r values, the medium-range features become more pronounced, and a peak $\sim$3.5 Å emerges.

The RMC model reproduces the first Mg-O peak at 2 Å including the tail at high-r values. The average Mg-O coordination number, calculated from the RMC model with a Mg-O cutoff distance of 2.6 Å, is $CN_{Mg-O} = 4.34$, which indicates a mixture of several sites. The distribution between $^{[4]}$Mg, $^{[5]}$Mg, and $^{[6]}$Mg sites gives 68.8%, 27.8%, and 3.4%, respectively, where the superscripts represent four-, five- or sixfold coordination. We can note that in the MD initial model, CN_{Mg-O} is higher (4.6), which indicates that fitting the diffraction data tends to decrease the coordination number and increase the proportion of $^{[4]}$Mg. The Si-Si, Si-Mg, and Mg-Mg PPDFs present a broad distribution, with a first peak at a similar distance of $\sim$3.1 Å.

RMC does not give a unique glass model structure. Starting from a MD configuration probably drives the RMC modeling to the nearest local minimum. Therefore, we must be careful to avoid over-interpretation. To overcome this weakness, we obtained an additional random configuration, using a hard-sphere Monte Carlo model generated in different steps.[39] Similar values are found for the Mg environment with an average coordination of 4.3, distributed between 61.9% $^{[4]}$Mg, 33.2% $^{[5]}$Mg, and 4.9% $^{[6]}$Mg sites (with cutoff of 2.6 Å). This allows for verification that RMC gives results independent of the starting configuration, especially concerning the Mg local environment.

V. DISCUSSION

A. Mg local environment

The Gaussian fits and the RMC model give a similar average Mg-O coordination number of 4.5 ± 0.1, corresponding to a

TABLE II. Gaussian parameters obtained by fitting the correlation functions. R, CN, and σ are the interatomic distance (± 0.002 Å), coordination number (± 0.05), and standard deviation (± 0.002 Å), respectively.

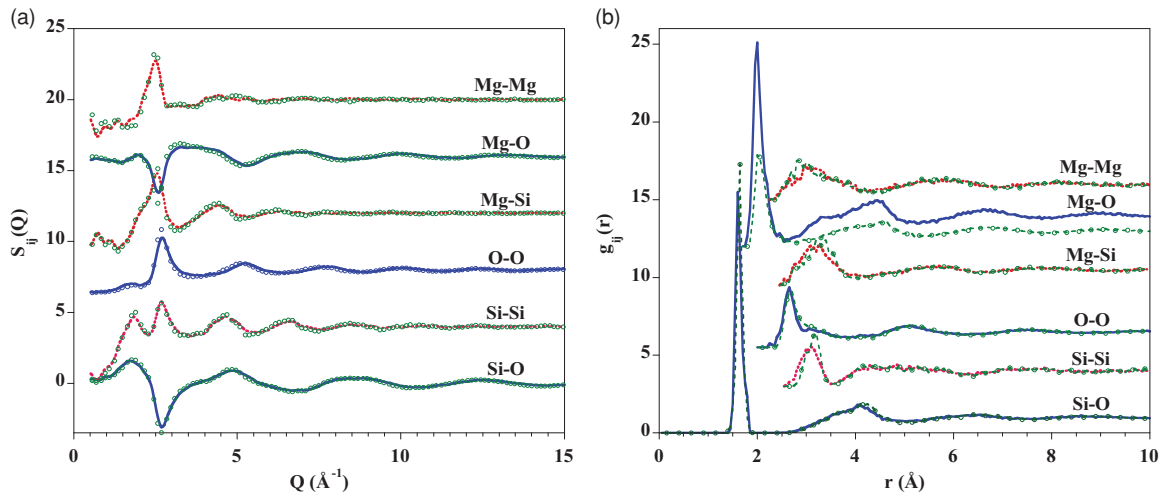|	R_{Si-O} (Å)	CN_{Si-O}	σ_{Si-O} (Å)	R_{Mg-O} (Å)	CN_{Mg-O}	σ_{Mg-O} (Å)	R_{Mg-O} (Å)	CN_{Mg-O}	σ_{Mg-O} (Å)
^{25}MgSiO$_3$	1.621	3.96	0.063	1.997	3.54	0.0865	2.21	0.98	0.08
^{nat}MgSiO$_3$	1.620	3.93	0.066	1.995	3.42	0.085	2.21	1.11	0.08
Diff.				1.995	3.42	0.085	2.21	1.11	0.08

FIG. 4. (Color online) (a) Partial structure factors $S_{ij}(Q)$ and (b) partial pair distribution functions $g_{ij}(r)$ calculated from the RMC model of the MgSiO₃ glass. The initial partial functions from the MD simulations are the dashed-dotted curves (green).

broad distribution of Mg-O bonds. This value is consistent with a recent investigation coupling neutron and x-ray diffraction data.[16] We can note that the coordination is lower than in our previous study, where the initial model suffers from a higher density than the experimental one.[17] A major result of our analysis is to distinguish two Mg-O contributions at ∼2 and 2.21 Å. Each contribution cannot unambiguously be attributed to a particular coordination site, as they are probably an overlap of the distances for the possible [4]Mg, [5]Mg, and [6]Mg sites. The first Mg-O contribution is intermediate between the average distances for [4]Mg (1.924 Å) and [6]Mg (∼2.10 Å).[40] The second Mg-O contribution is compatible with the highest distances for [5]Mg and [6]Mg found in silicate crystals.

Rather than a distorted coordination polyhedron with a broad distribution of Mg-O bond distances, the two Mg-O contributions reflect the presence of several coordination sites for Mg in MgSiO₃. According to the RMC model, which is strongly constrained by the $\Delta F^{\rm Mg}(Q)$ function that was unavailable previously, the Mg atoms are in the majority localized in small tetrahedral sites (68.8%) with a high proportion of fivefold coordinated sites (27.8%), while the amount of sixfold coordinated sites is small (3.4%). By starting with a random configuration, small changes are given in the different proportions: 62%, 33%, and 5% for [4]Mg, [5]Mg, and [6]Mg, respectively. The difference is an indication of the difficulties of resolving the different sites, which necessarily happens with strong overlapping. However, the general trend is a majority of [4]Mg, a high amount of [5]Mg, and some minor content of [6]Mg. The high proportion of [4]Mg suggests that an important amount of Mg can act as a network former. As previously noted,[41,42] a distribution of four- and fivefold coordinated sites for Mg is similar to the environments found for Fe²⁺ and Ni²⁺,[43,44] suggesting a close behavior for these cations.

In an early x-ray diffraction study, it was proposed that the Mg coordination in the MgSiO₃ glass can be considered as the sum of two very close coordination shells with four oxygen atoms at 2.08 Å and two other oxygen atoms at 2.5 Å, giving an octahedral coordination.[10] Our results agree

with the two distributions of Mg-O distances, but we have a different interpretation because an octahedral environment is not supported by our diffraction data. The coordination number is strongly dependent on the cutoff distance chosen. In Fig. 5, we plotted the evolution of the average Mg coordination number $CN_{\rm Mg}$ and the distribution of the different Mg sites as a function of the cutoff distance calculated from the RMC model. Between 2.5−2.7 Å, the $CN_{\rm Mg}$ number is almost constant. In order to increase $CN_{\rm Mg}$ up to 6, as suggested using the ²⁵Mg NMR data,[14,15] a cutoff distance of 3.2 Å has to be considered. This would imply extreme distortion of polyhedra and there is no justification to include high Mg-O bounds in the first coordination shell. Furthermore, the $\Delta D^{\rm Mg}(r)$ function [Fig. 2(b)] clearly shows a minimum at 2.5 Å. This reveals that there is no distribution of Mg-O distances above 2.5 Å as would be expected for distorted polyhedra. The implication is that the Mg sites are very well defined though distorted, which yields the tail at high-r values. An inspection of [4]Mg and [5]Mg sites in the RMC model reveals that both tetrahedral and pentahedral configurations present distortions, with usually one elongated Mg-O distance responsible for the high-r-side tail.

The Mg coordination is likely strongly composition dependent. Cs-, Rb- and K-bearing silicate glasses favor [4]Mg,
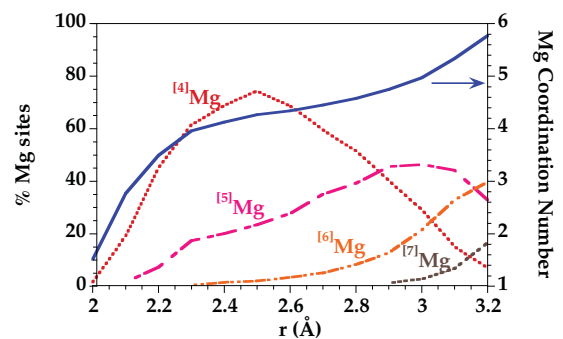

FIG. 5. (Color online) Evolution with the Mg-O cutoff distance of the average coordination number (right) and the distribution of Mg sites (left).

while Ca-, Na-, and Li-bearing silicate glasses favor [5]Mg or distorted [6]Mg.[13,15,41,45] In aluminosilicate glasses, [5]Mg sites are dominant.[40,41,46] An increase from 4 to 5 is also observed in the MgO-SiO$_2$ binary as the MgO content increases up to the Mg$_2$SiO$_4$ composition, leading to the formation of a highly distorted magnesium framework.[11,16] The coordination change between MgSiO$_3$ (enstatite) and Mg$_2$SiO$_4$ (forsterite) compositions could reflect a change in the magnesium structural role when going from a glass based on a silicate network (enstatite) to a glass where magnesium polyhedral linkages dominate (forsterite). On the contrary, [25]Mg NMR studies indicate [6]Mg in the MgSiO$_3$-Mg$_2$SiO$_4$ system, without any coordination change.[13,14]

Mg is mostly encountered in silicate crystals in [6]Mg sites and especially in enstatite MgSiO$_3$ and in forsterite Mg$_2$SiO$_4$. [4]Mg is observed in åkermanite with a Mg-O distance of 1.918 Å,[47] or in a potassium magnesiosilicate crystal with a Mg-O distance of 1.955 Å.[48] [5]Mg is found in yoderite with an average Mg-O distance of 2.016 Å,[49] and grandidierite with a distribution of Mg-O distance between 1.96−2.18 Å.[50] The low coordination found in the MgSiO$_3$ glass is thus unusual for the crystalline state. The structure of proto-enstatite (the high temperature stable form of MgSiO$_3$) shows an interesting aspect in its Mg environment. One Mg site is almost a regular octahedron (Mg-O distances at 2.0, 2.1, and 2.2 Å) but the second Mg site is strongly distorted, with four oxygens at 2.1 Å and two other oxygens at 2.5 Å. Although in our case, the presence of [6]Mg is small, this crystalline example shows the possibility of having strongly distorted polyhedra with long Mg-O bonds. In the proto-enstatite structure, this Mg-O distance corresponds to an oxygen already bounded with two SiO$_4$ tetrahedra, thus satisfying the bond valence requirement. As a result, the Mg-O distance is elongated to avoid an important excess of charge on this oxygen. A similar interpretation of the distortion of Mg polyhedra in the MgSiO$_3$ glass can be proposed. It is also noteworthy that the two longer bonds in proto-enstatite increase considerably with temperature (up to 2.8 Å at 1200 K).[51] Recent x-ray diffraction data have been obtained in the liquid state for MgSiO$_3$,[52] showing a higher degree of disorder around magnesium. However, the Mg coordination number is not changed at 2300 K. This lack of coordination change between the liquid and the glass suggest that the structure of MgSiO$_3$ and its magnesium environment are inherited from the liquid. It was also shown in a CaMgSi$_2$O$_6$ diopside glass that Mg remains coupled to the silicate network motion at low temperature,[53] contrary to alkalis or Ca.[53,54] This implies a strong bonding of Mg with the silicate network and this is in good agreement with a network-forming role.

B. Relation with the silicate network

If we consider a bridging O as an O bounded to two Si, we can determine in the RMC model the distribution of Q^n species, with n being the number of BO per SiO$_4$ tetrahedra (Table III). The silicate network appears to be composed mainly of Q^2 units, with the remaining Si being distributed between Q^1 and Q^3 units. These values are in excellent agreement with those reported using ^{29}Si Magic Angle Spinning NMR.[55] The high number of Q^2 units results

TABLE III. Percentages of Q^n species as calculated in the RMC model or obtained from ^{29}Si MAS NMR (Ref. 55).

	Q^0	Q^1	Q^2	Q^3	Q^4
RMC model	4.0	19.5	35.75	28.75	12.0
^{29}Si NMR	0.0	25.0	42.0	25.7	7.3

from the large amount of MgO that depolymerizes the silicate network with the formation of nonbridging oxygens (NBOs). These NBOs represent 62.7% of the total O atoms. From the Q^n distribution, we can calculate a number of NBOs per SiO$_4$ tetrahedra, NBO/Si = $\sum x_n(4\text{-}n)$ (where x_n is the fraction of each Q^n species) equal to 1.75. This value is smaller than that of 2 predicted by the stoichiometry. The discrepancy implies a high proportion of Q^3 and Q^4 units, which shifts the NBO/Si ratio to lower values, increases the silicate connectivity, and reduces the number of NBOs. To compensate for this high connectivity, the formation of oxygen not bounded to any Si atoms, i.e., "free" oxygen,[14] is required. In our RMC model, we have ∼4.6% of total O that are free oxygens. These species are associated either with [4]Mg or [5]Mg sites. The consequence of high connectivity and the presence of free oxygens is the increase in the heterogeneity of the network with high silicate connected regions and regions with free oxygens associated with Mg (see below).

In the RMC model, the $g_{MgSi}(r)$ PPDF presents a first peak at 3.1−3.2 Å. This corresponds to Mg polyhedra corner shared with SiO$_4$ tetrahedra, while edge linkages are observed between two Mg polyhedra. A significant fraction of O (30%) forms triclusters (O shared by three tetrahedra), being bounded mostly to one SiO$_4$ and two MgO$_4$ tetrahedra. The existence of these triclusters is required for a charge-balancing argument. If we consider the Pauling bond strength of Mg-O (0.5 u.v.) and Si-O (1 u.v.), an oxygen will be in an electrostatic stable environment if the sum of its bond strength equal its charge, which is 2. Therefore, this imposes two Mg-O bonds and one Si-O bond (three linked MgO$_4$ tetrahedra implies O underbonding and three linked SiO$_4$ tetrahedra gives strong overbonding).

C. Mg distribution

The $g_{MgMg}(r)$ PPDF exhibits a first broad contribution centered at 3.1 Å. Additional Mg-Mg contributions are discernible at 5.8 and 8.3 Å, and a very weak contribution is found at 10.6 Å. The short first Mg-Mg distance is an indication of the direct linkages between Mg polyhedra. An inspection of the RMC model reveals mainly corner sharing and a minority of edge-sharing linkages. A similar study has been carried out on a CaSiO$_3$ glass using NDIS to obtain a second difference function,[25] which is a technique that has been used for a limited number of cation in silicate glasses.[56] Ca-Ca distances were determined at 3.8 and 6.4 Å, which was interpreted as corrugated sheets of CaO$_6$ octahedra presenting important similarities with the arrangements found in the crystalline counterpart. MD simulations of the CaSiO$_3$ glass can reproduce these distances but conclude either to clustered Ca domains, rather than layered domains,[21] or to the absence of any cation ordering.[57] MD simulations and RMC
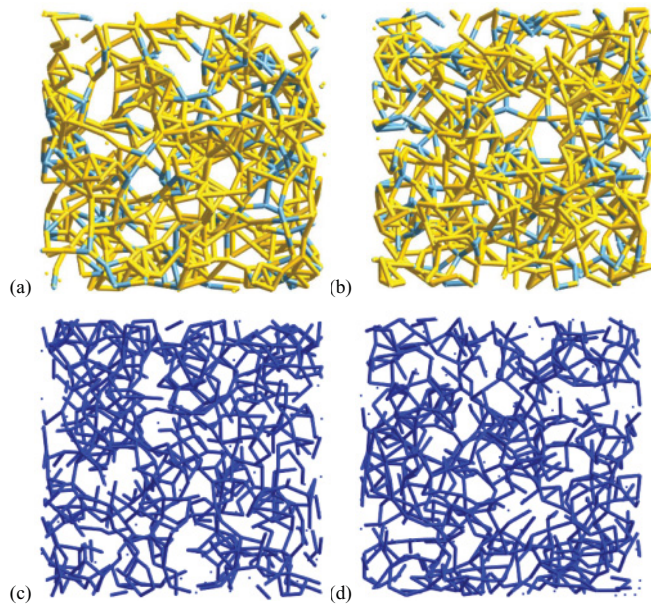
FIG. 6. (Color online) Different projections of the RMC model: (a), (b) the Mg distribution with yellow bonds starting from [4]Mg sites and blue bonds starting from [5]Mg and [6]Mg sites, and (c), (d) the Si distribution. Cutoff distances are 4.2 Å and 3.5 Å for Mg-Mg and Si-Si bonds, respectively.

modeling usually gives structure with a low degree of order, resulting from the intrinsic characteristics of these methods. The shorter Mg-Mg distances compared to the Ca-Ca ones reflect the difference in cation size and the lower coordination of Mg compared to Ca, which occurs mainly in octahedral sites.[25] In Fig. 6, the Mg distribution in the RMC model is represented with the direct Mg-Mg linkages using a cutoff of 4.2 Å [first minimum in the $g_{MgMg}(r)$ PPDF]. Although a two-dimensional representation of a three-dimensional structure can be biased due to thickness integration, we observe that the Mg distribution does not appear homogeneous. It is possible to identify regions where Mg atoms tend to segregate,

which correspond to regions with lower concentrations of Si. According to the $g_{MgMg}(r)$ PPDF, the inhomogeneous regions correspond to medium-range ordering extending to ∼1 nm. They could prefigure the structural organization in Mg$_2$SiO$_4$ glass where a Mg network dominates. The Mg distribution is interesting to better understand the structural role of this cation within the structure. For a simple network forming role of Mg, substituting to Si, we would expect a random substitution, as observed for the Al substituted to Si in aluminosilicate glasses.[58] The inhomogeneous Mg distribution is thus an indication that Mg does not simply substitute to Si in tetrahedral sites, but forms its own network where high coordinated sites are required to ensure local electroneutrality and stabilization of the structure. Furthermore, inhomogeneities will promote the extensive immiscibility gap observed along the MgO-SiO$_2$ binary and explain the difficulties in obtaining a glassy state.

VI. CONCLUSIONS

To summarize, a combination of neutron and x-ray diffraction coupled with reverse Monte Carlo modeling has been used to study the structure of MgSiO$_3$ glass. Performing neutron-diffraction isotopic substitution, we have separated the pair distribution functions associated with Mg from the silicate network, allowing an accurate and unambiguous determination of the Mg environment. The detailed description of the Mg environment gives a broad distribution of Mg-O bonds at 2 with a tail at 2.21 Å, and an average coordination number for Mg of 4.5 ± 0.1. RMC modeling confirms these results and indicates a majority of fourfold coordinated sites and a minority of fivefold coordinated sites. Both sites appear distorted, which explains the broad distribution of Mg-O distances. Adding an additional O will lead to excessive polyhedral distortion and to Mg-O distances exceeding 3.0 Å. The network appears inhomogeneous with Si-enriched regions, which explains the high proportion of Q^3 and Q^4 species and Mg-enriched regions. This organization could prefigure that of invert glasses and is close to that expected for the corresponding melts.

*cormier@impmc.upmc.fr

[1] A. Pedone, M. Malavasi, C. Menziani, U. Segre, and A. N. Cormack, J. Phys. Chem. C **112**, 11034 (2008).

[2] E. Jallot, Appl. Surf. Sci. **211**, 89 (2003).

[3] A. Pedone, M. Malavasi, and C. Menziani, J. Phys. Chem. C **113**, 15723 (2009).

[4] J. Kraxner *et al.*, *in Glass – the Challenge for the 21st Century*, edited by M. Liska, D. Galusek, R. Klement and V. Petruskova (Trans Tech, Stafa-Zurich, 2008), Vol. 39–40, p. 81.

[5] F. R. Schilling *et al.*, Contr. Miner. Petrol. **141**, 297 (2001).

[6] C.-C. Lin, S.-F. Chen, L.-G. Liu, and C.-C. Li, J. Non-Cryst. Solids **353**, 413 (2007).

[7] G. R. Helffrich and B. J. Wood, Nature (London) **412**, 501 (2001).

[8] F. J. Molster *et al.*, Nature (London) **401**, 563 (1999).

[9] J. Dorschner *et al.*, Astron. Astrophys. **300**, 503 (1995).

[10] C. D. Yin *et al.*, J. Non-Cryst. Solids **55**, 131 (1983).

[11] S. Kohara, K. Suzuya, K. Takeuchi, C.-K. Loong, M. Grimsditch, J. K. R. Weber, J. A. Tangeman, and T. S. Key, Science **303**, 1649 (2004).

[12] T. Taniguchi, M. Okuno, and T. Matsumoto, J. Non-Cryst. Solids **211**, 56 (1997).

[13] K. Shimoda, Y. Tobu, M. Hatakeyama, T. Nemoto, and K. Saito, Am. Mineral. **92**, 695 (2007).

[14] S. Sen, H. Maekawa, and G. N. Papatheodorou, J. Phys. Chem. B **113**, 15243 (2009).

[15] K. Shimoda, T. Nemoto, and K. Saito, J. Phys. Chem. B **112**, 6747 (2008).

[16] M. C. Wilding, C. J. Benmore, J. A. Tangeman, and S. Sampath, Chem. Geol. **213**, 281 (2004).

[17] M. Guignard and L. Cormier, Chem. Geol. **256**, 111 (2008).

[18] M. C. Wilding, C. J. Benmore, and J. K. R. Weber, J. Mater. Sci. **43**, 4707 (2008).

[19] Y. Matsui and K. Kawamura, Nature (London) **285**, 648 (1980).

[20]J. D. Kubicki and A. C. Lasaga, Phys. Chem. Minerals **17**, 661 (1991).

[21]K. Shimoda and M. Okuno, J. Phys.: Condens. Matter **18**, 6531 (2006).

[22]L. Cormier, S. Creux, L. Galoisy, G. Calas, and P. H. Gaskell, Chem. Geol. **128**, 77 (1996).

[23]L. Cormier, G. Calas, and P. H. Gaskell, Chem. Geol. **174**, 349 (2001).

[24]M. C. Eckersley, P. H. Gaskell, A. C. Barnes, and P. Chieux, Nature (London) **335**, 525 (1988).

[25]P. H. Gaskell *et al.*, Nature (London) **350**, 675 (1991).

[26]H. E. Fischer *et al.*, Appl. Phys. A **74**, S160 (2002).

[27]D. A. Keen, Appl. Crystallogr. **34**, 172 (2001).

[28]C. Weigel, L. Cormier, G. Calas, L. Galoisy, and D. T. Bowron, Phys. Rev. B **78**, 064202 (2008).

[29]G. J. Cuello, J. Phys.: Condens. Matter **20**, 244109 (2008).

[30]F. Marumo and M. Okuno, in *Materials Science of the Earth's Interior*, edited by I. Sunagawa (Terra Scientific, Tokyo, 1984), p. 25.

[31]M. Guignard, L. Cormier, V. Montouillout, N. Menguy, and D. Massiot, J. Non-Cryst. Solids **356**, 1368 (2010).

[32]A. C. Wright, in *Advances in Structure Research by Diffraction Methods, edited by W. Hoppe and R. Mason* (Pergamon, Oxford, 1974), Vol. 5, p. 1.

[33]M. Guignard *et al.*, J. Phys.: Condens. Matter **21**, 375107 (2009).

[34]L. Cormier, D. Ghaleb, J. M. Delaye, and G. Calas, Phys. Rev. B **61**, 14495 (2000).

[35]W. Smith and T. R. Forester, J. Mol. Graphics **14**, 136 (1996).

[36][http://www.ccp5.ac.uk/DL_POLY/].

[37]B. Guillot and N. Sator, Geochim. Cosmochim. Acta **71**, 1249 (2007).

[38]R. L. McGreevy and L. Pusztai, Mol. Sim. **1**, 359 (1988).

[39]R. L. Mc Greevy and P. Zetterström, J. Non-Cryst. Solids **293–295**, 297 (2001).

[40]D. Li, M. S. Peng, and T. Murata, Can. Mineral. **37**, 199 (1999).

[41]N. Trcera, D. Cabaret, S. Rossano, F. Farges, A.-M. Flank, and P. Lagarde, Phys. Chem. Minerals **36**, 241 (2009).

[42]P. S. Fiske and J. F. Stebbins, Am. Mineral. **79**, 848 (1994).

[43]S. Rossano, A. Y. Ramos, and J.-M. Delaye, J. Non-Cryst. Solids **273**, 48 (2000).

[44]L. Galoisy and G. Calas, Geochim. Cosmochim. Acta **57**, 3613 (1993).

[45]S. Kroeker and J. F. Stebbins, Am. Mineral. **85**, 1459 (2000).

[46]P. Ildefonse *et al.*, Nucl. Instrum. Methods **97**, 172 (1995).

[47]I. P. Swainson *et al.*, Phys. Chem. Minerals **19**, 185 (1992).

[48]A. A. Khan, W. H. Baur, and W. C. Forbes, Acta Crystallogr. B **28**, 267 (1972).

[49]J. B. Higgins, P. H. Ribbe, and Y. Nakajima, Am. Mineral. **67**, 76 (1982).

[50]D. A. Stephenson and P. B. Moore, Acta Crystallogr. B **24**, 1518 (1968).

[51]H. Yang and S. Ghose, Am. Mineral. **80**, 9 (1995).

[52]M. C. Wilding, C. J. Benmore, and J. K. R. Weber, Europhys. Lett. **89**, 26005 (2010).

[53]A. M. George and J. F. Stebbins, Am. Mineral. **83**, 1022 (1998).

[54]G. Gruener, P. Odier, D. DeSousa Meneses, P. Florian, and P. Richet, Phys. Rev. B **64**, 24206 (2001).

[55]P. Zhang, P. J. Grandinetti, and J. F. Stebbins, J. Phys. Chem. B **101**, 4004 (1997).

[56]L. Cormier, L. Galoisy, J.-M. Delaye, D. Ghaleb, and G. Calas, C. R. Acad. Sci. Ser. IV-Phys. Astrophys. **2**, 249 (2001).

[57]R. N. Mead and G. Mountjoy, J. Phys. Chem. B **110**, 14273 (2006).

[58]S. K. Lee and J. F. Stebbins, J. Non-Cryst. Solids **270**, 260 (2000).